Disturbance Observer-Based Hybrid Control of Displacement and Force in a Medical Tele-Analyzer

Anan Suebsomran and Manukid Parnichkun*

Abstract: This paper presents hybrid control of displacement and force in a Medical Tele-Analyzer by disturbance observer-based controller which is robust to internal and external disturbances; model uncertainty, load, and friction for instances. The developed Medical Tele-Analyzer consists of 2 subsystems; doctor-side subsystem and patient-side subsystem. In the doctor side subsystem, an array of displacement sensor is equipped to detect movement of doctor's hand and fingers. The detected information is transmitted to the patient side to be used in medical analysis. On the other hand, the patient-side subsystem consists of an array of displacement actuators, which is used to follow displacement of doctor's hand and fingers. An array of force sensors is used to detect forces between patient and the equipment. Since displacement control in patient side is coupled with force control in doctor side and vice-versa, design of the controller has to take into account this coupling. Not only using in medical tele-analysis, the proposed system can also be used in any tele-displacement-force controls of industrial processes.

Keywords: Disturbance observer, hybrid control of displacement and force, robust control, medical tele-analyzer.

1. INTRODUCTION

Nowadays only audio and vision sensations are transmittable remotely and used in Medical Tele-Analysis. Transmission of tactile sensation is still under investigation. There are many difficulties in tactile transmission including regeneration of tactile sensation. This paper states in general about a Medical Tele-Analyzer, which is being developed at Mechatronics and Automation laboratory, AIT [6-8]. This equipment is used to analyze abnormal mass on abdomen remotely; e.g. hepatomegaly, splenomegaly. It can be applied in the case where medical doctors cannot approach patients directly; for examples in the case when expert medical doctors are far away from patients or in the case of heavy infection.

The developed Medical Tele-Analyzer consists of 2 subsystems; doctor-side subsystem and patient-side subsystem as shown in Fig. 1. In the doctor-side subsystem, an array of 80 units displacement sensor is equipped to detect movement of doctor's fingers and hand. The detected information is transmitted to the patient-side subsystem. An array of 80 units force actuator is used to generate forces detected at the patient side to be used in abdominal mass analysis. On the other hand, the patient-side subsystem consists of an array of 80 units displacement actuator which is used to follow movement of doctor's fingers and hand. An array of 80 units force sensor is used to detect forces between patient and the equipment.

Not only using in medical tele-analysis, the proposed system can also be used in any tele-displacement-force controls of processes.

Disturbance observer-based controller, which is robust to internal and external disturbances; model uncertainty, load, and friction for instances, is applied here to control both displacement and force. Since displacement control in patient side is coupled with force control in doctor side and force control in doctor side is coupled with displacement in patient side, design of the controller has to take into account this coupling.

2. HARDWARE ARCHITECTURE

2.1. Displacement sensors and actuators

Resistive potentiometers are applied to detect current positions of active cells in the doctor-side subsystem pressed by doctor's fingers and hand. The sensing range of 40 mm and resolution of 2 mm,

Manuscript received August 27, 2004; accepted January 28, 2005. Recommended by Editorial Board member Eun Tai Kim under the direction of Editor Keum-Shik Hong. This research is financially supported by National Electronics and Computer Technology Center (NECTEC), National Science and Technology Development Agency (NSTDA).

Anan Suebsomran and Manukid Parnichkun are with the School of Advanced Technologies, Asian Institute of Technology, P.O.Box 4, Klongluang, Pathumthani 12120, Thailand (e-mails: {anan.suebsomran, manukid}@ait.ac.th).
* Corresponding author.

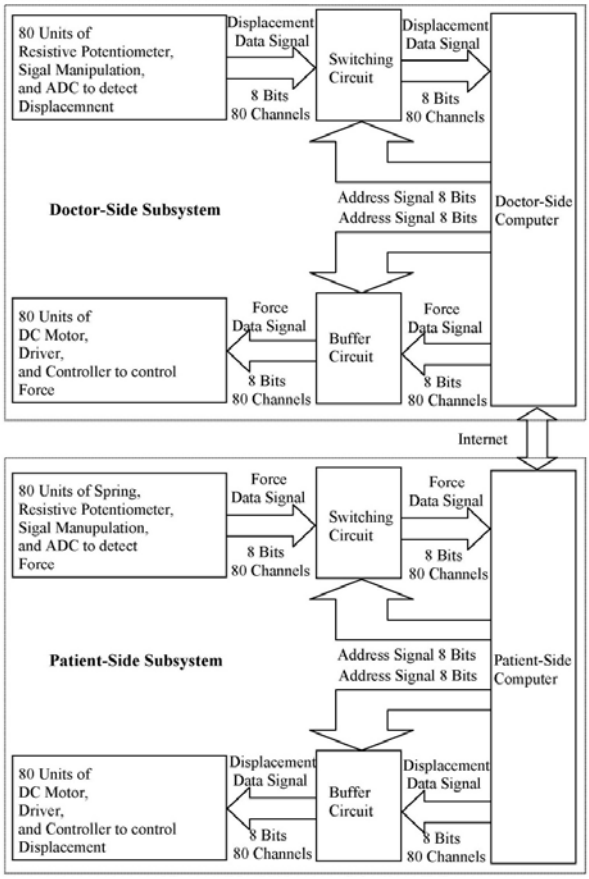

Fig. 1. Block diagram of the overall system.

which are the practical dimensions in abdomen pressing in mass analysis, are criteria of potentiometer selection. The 10 kΩ resistive potentiometers used to detect displacements are made from carbon with metal frame of the dimension 12x88x11 mm and 62 mm moving stroke. The information is then converted to digital form by ADC before being transmitted to the patient-side subsystem.

Responding to displacement information sent from the doctor-side subsystem, DC motors are applied to generate displacements of active cells in the patient-side subsystem.

2.2. Force sensors and actuators

Force sensors made from potentiometers and springs are applied to detect current resultant forces on active cells in the patient-side subsystem resulted from pressing active cells on patient's abdomen. The sensing range of 4725 g, which is the practical maximum force in abdomen pressing in abdominal mass analysis, and the resolution of 20 g are criteria of force sensor. The 100 kΩ resistive potentiometers used to detect forces are made from carbon with metal frame of the dimension 10x35x6 mm and 20 mm moving stroke. Coil springs with 1 mm coil diameter and 13 spring external diameter and 30 mm length and 2.45 N/mm spring constant are used in combination

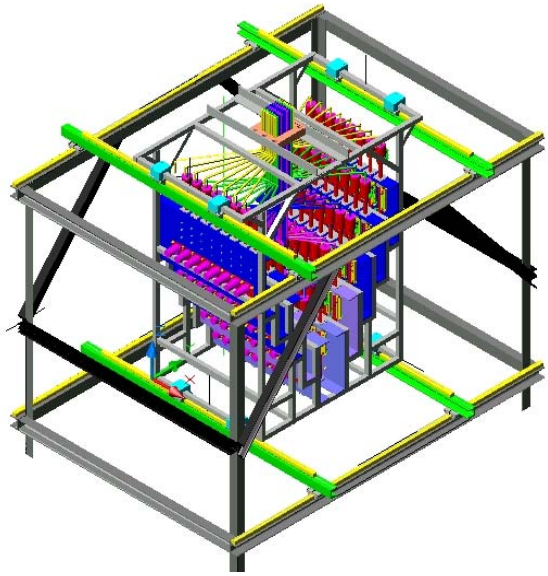

Fig. 2. Doctor-side subsystem.

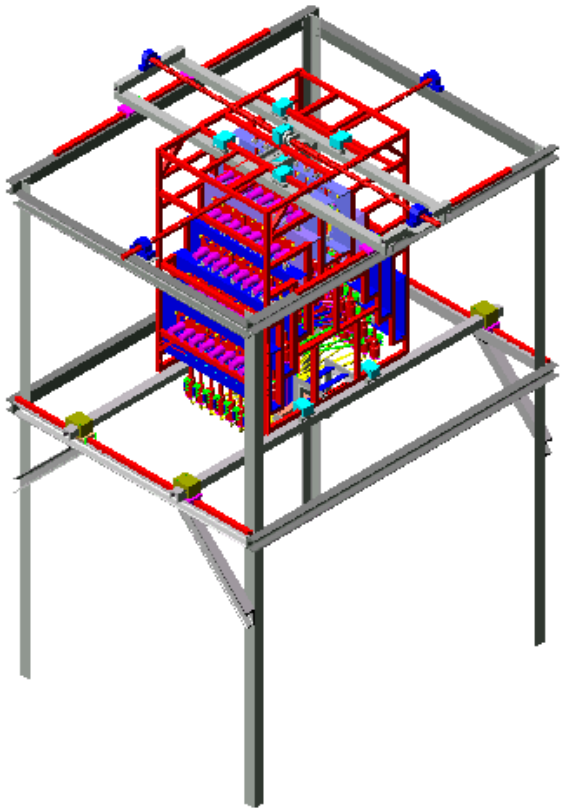

Fig. 3. Patient-side subsystem.

with resistive potentiometer in order to detect forces. The detected force information is then converted to digital form by ADC before being transmitted to the doctor-side subsystem.

Responding to force information sent from the patient-side subsystem, DC motors are applied to generate forces reacting to the doctor's fingers and hand.

2.3. Hardware prototype

Hardware prototype of the displacement-force controlled medical tele-analyzer was developed. The doctor-side subsystem is depicted in Fig. 2 whereas the patient-side subsystem is depicted in Fig. 3.

2.4. Motor parameters identification

Many experiments were conducted in order to identify motors parameters. The results of identification are shown below.

Parameters	Description	Values	Units
J_n	Nominal Inertia	0.000254	Kg.m^2
K_{tn}	Nominal Torque Constant	0.1656	N.m/A
C	Damping Constant	0.002031	N.m.s/rad
K_e	Back EMF Constant	0.982	V.s/rad
R	Armature Resistance	26.44	Ω
L	Armature Inductance	0.0138	H

3. COMMUNICATION AND TELE-ANALYSIS

A well-known client-server on TCP/IP is used as a communication protocol to exchange information between doctor-side and patient-side subsystems. TCP/IP supports both LAN system for internal use and telephone-line system for external use. Flowchart of the client-server on TCP/IP networking by using Winsock is shown in Fig. 4.

The procedure to establish communication in the server side starts from creating a socket. The socket is then bound to a specific port. Listen is the step to indicate willingness to accept incoming connection request. Then the server waits for incoming request. During data exchange, the server can either send or receive data. Communication is terminated by closing the opened socket.

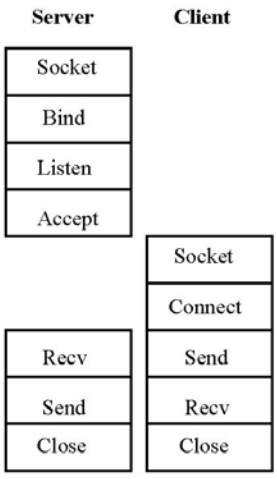

Fig. 4. Flowchart of client-server on TCP/IP networking.

The procedure to establish communication in the client side also starts from creating a socket. The client then initiates a connection to a specific server. Similarly, during data exchange, the client can either send or receive data also. Communication is terminated by closing the opened socket.

Connection between computer and controller in each subsystem is done via PCI bus, whereas, connection between sensors/actuators and microprocessor is done via parallel ports.

Current displacement and force of each active cell are displayed on the doctor-side subsystem for analysis. The analysis of abdominal mass is done by the consideration of contours of magnitudes of displacement and force displayed on the monitor. These contours are collected and used as inputs in the training process. The contours are also used to search for the highest match one in the analysis process.

The communication software was developed on Microsoft Visual C++ applying Winsock class, whereas, the graphic output was developed on Microsoft Visual C++ applying Open GL class.

4. DISTURBANCE OBSERVER-BASED CONTROLLER

In motion control system, servomechanism needs self-tuning to adjust dynamics and kinematics of the system. This self-tuning has to compensate effects of internal and external disturbances; model uncertainty, load, and friction for instances. Normally, the controlled system consists of a plant and a controller, which is used to shape both transient and steady-state responses of the controlled plant to the desired characteristics. Robust motion control is needed to control the plant in the environment where model uncertainty, and disturbances exists. Disturbance observer-based controller, which generates the acceleration signal to the plant is a robust controller and proposed to be applied in the developed medical tele-analyzer. All plants always act to some loads. Torque generated from load is treated as a disturbance in disturbance observer-based controller. The controller can compensate the disturbance by using disturbance observer technique as shown in block diagram in Fig. 5 [5].

In the diagram, J_n represents nominal inertia of the motor system, whereas, J represents the actual inertia. K_{tn} represents nominal torque constant of the motor system, whereas, K_t represents the actual torque constant. Both J and are unknown and

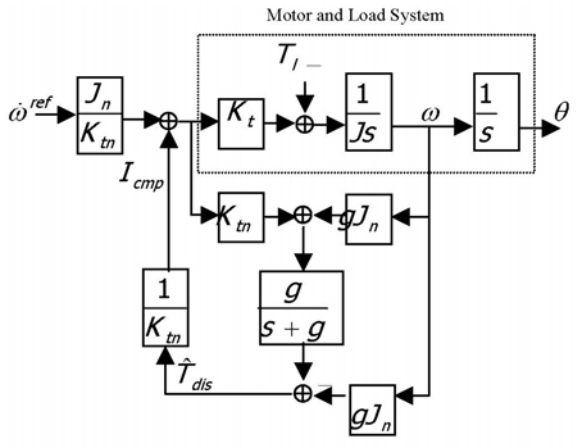

Fig. 5. Disturbance observer-based controller.

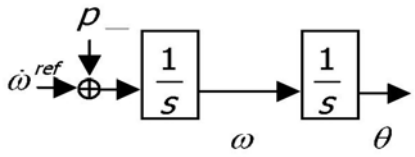

Fig. 6. Equivalent block diagram.

depend on many factors. In contrary, both J_n and K_{tn} are known parameters. The system in the dotted area in Fig. 5 indicates the actual motor and load system. The function of $g/(s+g)$ in the diagram is to attenuate high frequency components resulting from differentiation action in the system.

Block diagram in Fig. 5 is equivalent to block diagram in Fig. 6. The DC motor model follows

$$J\frac{d\omega}{dt} = K_t I_a - (T_{int} + T_{ext} + T_{frc}), \tag{1}$$

when T_{int} is inertia torque, T_{ext} is external torque, and T_{frc} is friction torque. By decomposing inertia and torque constant of the motor, (1) becomes

$$(J_n + \Delta J)\frac{d\omega}{dt} = (K_{tn} + \Delta K_t)I_a - (T_{int} + T_{ext} + T_{frac}). \tag{2}$$

By rewriting (2)

$$J_n\frac{d\omega}{dt} = K_{tn}I_a - (T_{int} + T_{ext} + T_{frac}) - \Delta J\frac{d\omega}{dt} + \Delta K_t I_a \tag{3}$$

and introduce disturbance torque, T_{dis} as

$$T_{dis} = T_{int} + T_{ext} + T_{frac} + \Delta J\frac{d\omega}{dt} - \Delta K_t I_a. \tag{4}$$

The DC motor model, thus, becomes

$$J_n\frac{d\omega}{dt} = K_{tn}I_a - T_{dis}. \tag{5}$$

From Fig. 5, the disturbance torque after passing low pass filter is

$$\hat{T}_{dis} = \frac{g}{s+g}T_{dis}. \tag{6}$$

In the diagram of Fig. 6, p represents the attenuated disturbance and it is equivalent with equation in (7)

$$p = \dot{\omega}^{ref} - \dot{\omega} = J_n^{-1}G_s T_{dis}, \tag{7}$$

where

$$G_s = \frac{s}{s+g}. \tag{8}$$

The sensitivity function, G_s, attenuates disturbance component which frequency is lower than g. For a unit step disturbance, p converges to 0 at the steady state. If g is selected high enough, effect of disturbance is negligible. In the other word, the disturbance is removed by the disturbance observer.

5. DISPLACEMENT-FORCE HYBRID CONTROL

There are two separated controllers in the medical Tele-analyzer; displacement and force controllers.

5.1. Displacement controller

Block diagram of displacement controller applying disturbance observe is illustrated in Fig. 7.
Displacement, thus, follows

$$x = x^{cmd} - \frac{x^{cmd}s^2 + p}{s^2 + k_d s + k_p}, \tag{9}$$

where k_p and k_d are used to shape the transient response. By similar reason, when g is high enough, p is negligible, and $x^{cmd}s^2$ converges to zero at steady state, thus x converges to x^{cmd} at steady state.

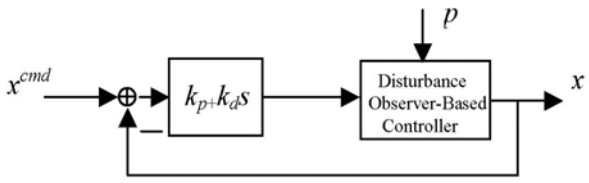

Fig. 7. Disturbance observer-based displacement controller.

5.2. Force controller

Block diagram of force controller applying disturbance observe is illustrated in Fig. 8.

Force, which is determined from

$$F = K_s x + Dxs \tag{10}$$

follows

$$F = F^{cmd} - M(xs^2 + k_d xs + p) \tag{11}$$

where k_d is used to shape the transient response. M, D, and Ks are mass, damping modulus, and spring constant respectively. By similar reason, when g is high enough, p is negligible, Mxs^2 and $Mk_d xs$ converges to zero at steady state, thus F converges to F^{cmd} at steady state.

6. SIMULATION AND EXPERIMENTAL RESULTS

Both experiment and simulation are done in order to verify performance of the controller. Parameters used in the simulation are set as followings:

Parameters	Description	Values	Units
J_n	Nominal Inertia	0.00025	Kg.m^2
J	Actual Inertia	0.0003	Kg.m^2
K_{tn}	Nominal Torque Constant	0.1656	N.m/A
K_t	Actual Torque Constant	0.2	N.m/A
C	Damping Constant	0.002031	N.m.s/rad
K_e	Back EMF Constant	0.982	V.s/rad
R	Armature Resistance	26.44	Ω
L	Armature Inductance	0.0138	H
M	System Mass	0.0003	Kg.m/rad
D	Damping Modulus	0	N.s/rad
K_s	Spring Constant	2.45	N/rad

6.1. Displacement control

Input applied to the system is a unit-step input as shown in Fig. 9, which represents displacement command. Gaussian random noise shown in Fig. 10 is put into the system to perform as disturbance. Mean of the gaussian random noise is set to 1 with variance of 0.25. By disturbance observer, the output can track the input without steady-state error as shown in Fig. 11. In the simulation, the gains k_p and k_d are adjusted to 500 and 100 respectively. Cutoff frequency of the LPF, performed by $g/(s+g)$, is set at 1000 rad/s.

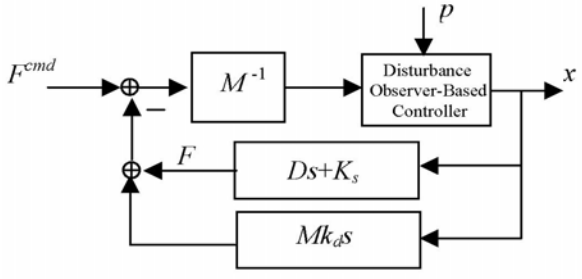

Fig. 8. Disturbance observer-based force controller.

Performance of disturbance observer-based controller is compared with the conventional PD controller as shown in Fig. 12. The gains kp and kd are also adjusted to 500 and 100. The output from PD controller is shown in Fig. 13. Steady-state error is detected in the response of PD controller.

The steady-state error of PD controller is analyzed and represented by

$$e_{ss} = -\frac{R}{K_t k_p}(T_{dis}). \tag{12}$$

The output is able to track the input properly, however, internal and external disturbances introduce error to the system at steady state. Fig. 14 shows steady-state error of the system by disturbance observer-based controller (*) and steady-state error of the system by PD controller (+) when mean of the disturbance varies from 0 to 10 N.m.

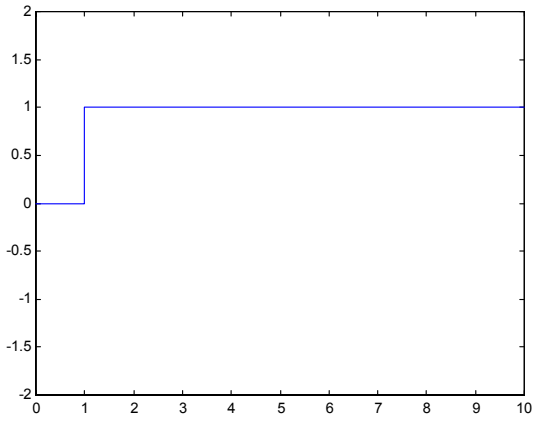

Fig. 9. Displacement command.

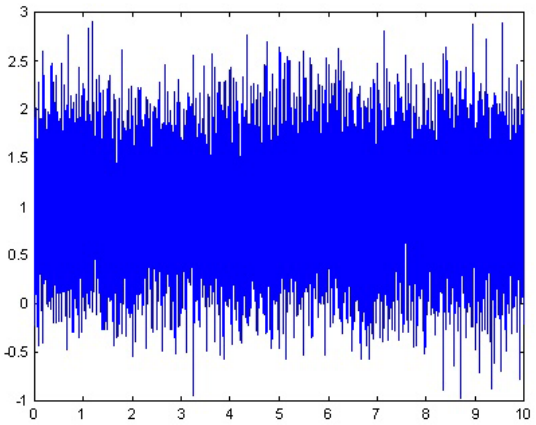

Fig. 10. Disturbance.

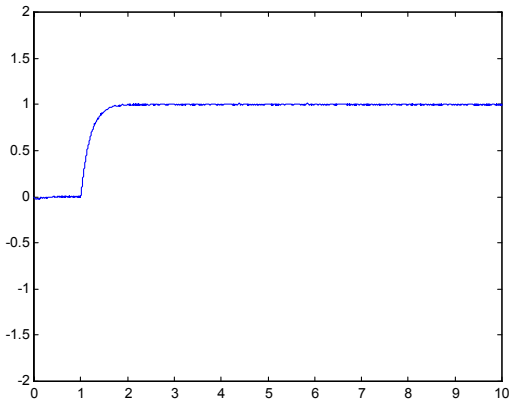

Fig. 11. Displacement response of disturbance observer-based controller.

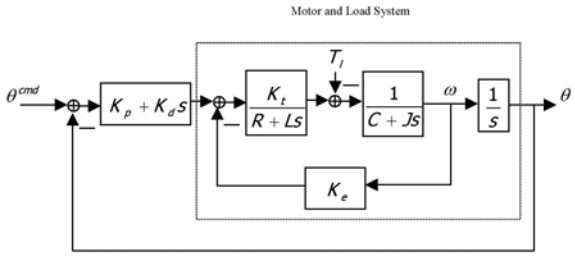

Fig. 12. PD displacement controller.

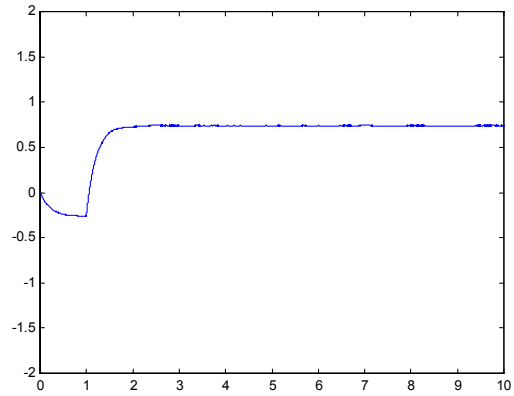

Fig. 13. Displacement response of PD controller.

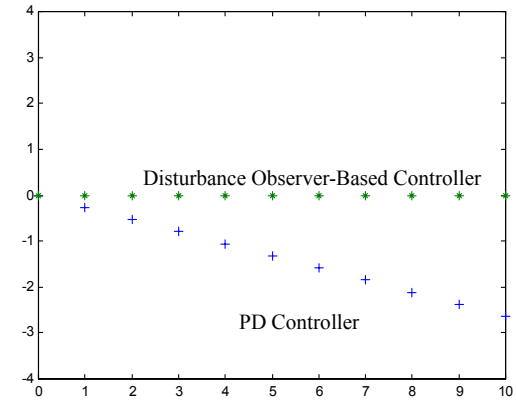

Fig. 14. Steady-state error of displacement.

Table 1. 100% rise time (milliseconds) of displacement response of 80 cells.

300	500	1100	1000	500	600	600	600
500	800	800	800	500	800	1200	500
300	500	400	800	1200	300	1000	800
400	400	500	1300	500	500	800	600
600	300	1000	1000	800	900	500	600
400	600	1000	400	300	600	400	1000
1200	500	1000	700	500	1000	500	300
1000	500	600	800	700	700	1200	1000
800	600	1000	800	800	600	500	400
300	500	800	300	1200	1100	300	600

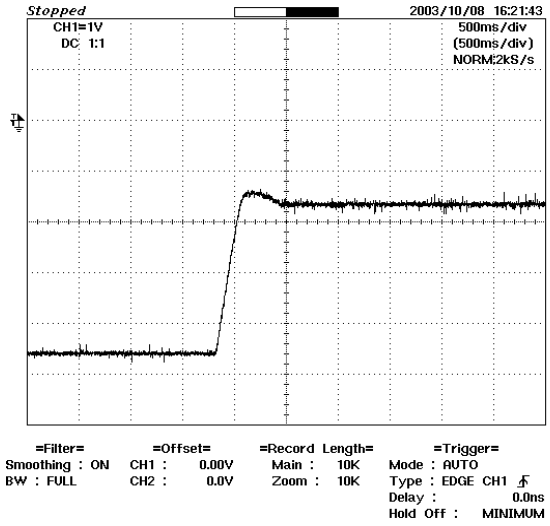

Fig. 15. Displacement response.

Experimental results of 100% rise time of displacement response of all the 80 cells are investigated and found at the average of 670 ms as shown in Table 1. Shape of the response is shown in Fig. 15.

6.2. Force control

Input applied to the system is a unit-step input as shown in Fig. 16, which represents force command. Gaussian random noise shown in Fig. 17 is put into the system to perform as disturbance. Mean of the gaussian random noise is set to 1 with variance of 0.25. By disturbance observer, the output can track the input without steady-state error as shown in Fig. 18. In the simulation, the gain kd is adjusted to 100. Cutoff frequency of the LPF, performed by g/(s+g), is set at 1000 rad/s.

Performance of disturbance observer-based controller is compared with the conventional PD controller as shown in Fig. 19. The gains kp and kd are adjusted to 500 and 100 respectively. The output from PD controller is shown in Fig. 20. Steady-state error is detected in the response of PD controller.

The steady-state error of PD controller is analyzed and represented by

$$e_{ss} = -\frac{R}{K_t k_p}(T_{dis}). \quad (13)$$

The output is able to track the input properly, however, internal and external disturbances introduce error to the system at steady state. Fig. 21 shows steady-state error of the system by disturbance observer-based controller (*) and steady-state error of the system by PD controller (+) when mean of the disturbance varies from 0 to 10 N.m.

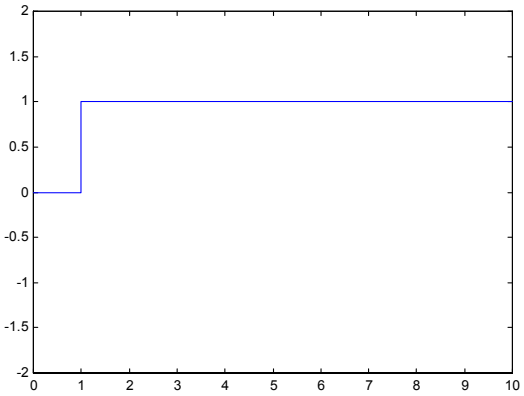

Fig. 16. Force command.

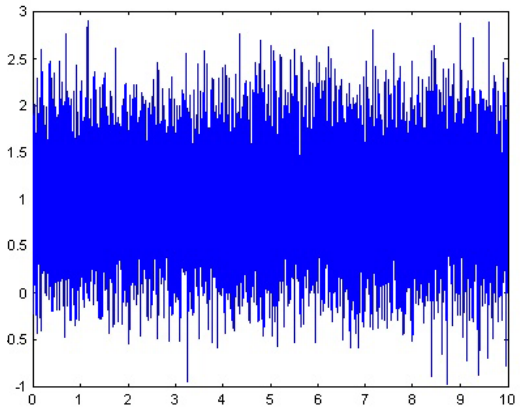

Fig. 17. Disturbance.

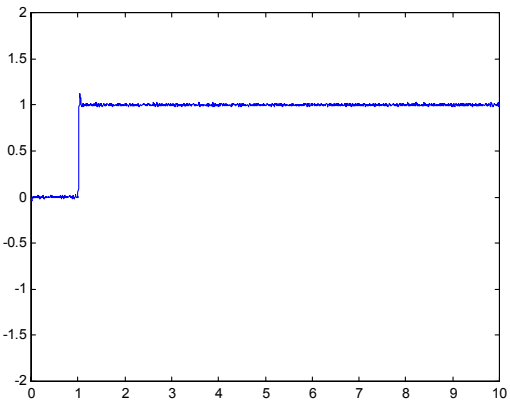

Fig. 18. Force response of disturbance observer-based controller.

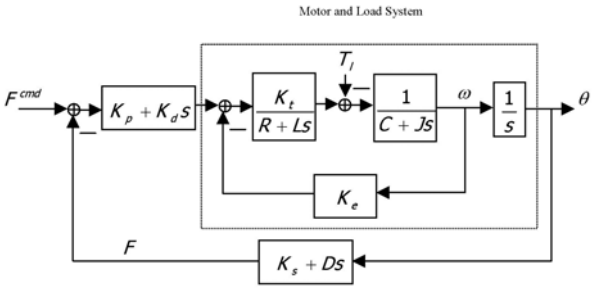

Fig. 19. PD force controller.

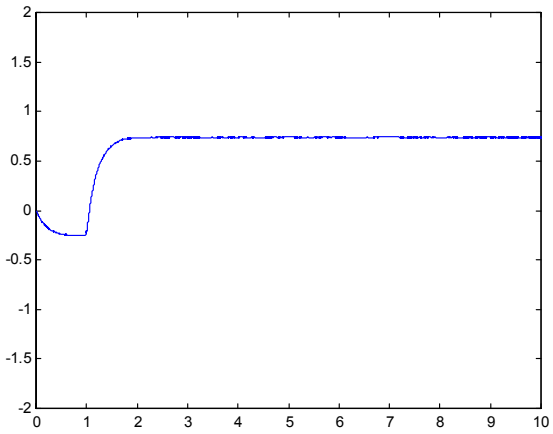

Fig. 20. Force response of PD controller.

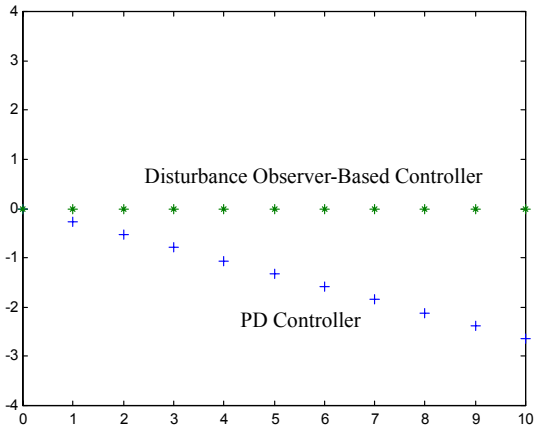

Fig. 21. Steady-state error of force.

Table 2. 100% rise time (milliseconds) of force response of 80 cells.

400	700	300	500	300	400	500	300
300	400	400	500	700	800	500	300
300	700	800	300	400	600	700	500
500	400	400	300	400	500	400	300
500	400	300	300	500	400	700	400
500	500	300	400	300	300	400	300
400	300	400	500	800	500	300	400
800	600	400	400	500	500	400	700
300	400	500	400	800	300	400	400
700	500	400	400	400	500	300	400

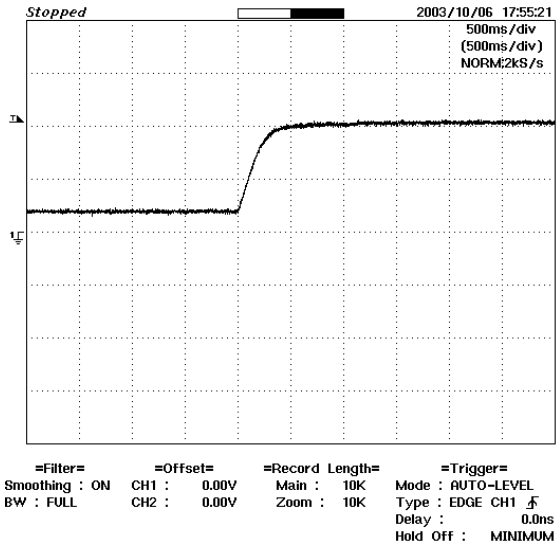

Fig. 22. Force response.

Experimental results of 100% rise time of force response of all the 80 cells are investigated and found at the average of 461.25 ms as shown in Table 2. Shape of the response is shown in Fig. 22.

6.3. Hybrid of displacement and force

The result of displacement and force control in hybrid scheme is explained in Figs. 23-25. Input shown in Fig. 23 is a step displacement command. Output is a force response, shown in Fig. 24 for disturbance observer-based controller, and shown in Fig. 25 for PD controller. Gaussian random noises are put into both displacement and force control loops to perform as disturbances. Means of the gaussian random noises are both set to 1 with variance of 0.25. In the simulation, conversion of magnitude from displacement to force is assumed to be 1 N/rad. From the results, hybrid control of displacement and force by disturbance-observer based controller is robust to disturbance, while PD is not robust to disturbance. The output responses show the combination result of displacement and force control.

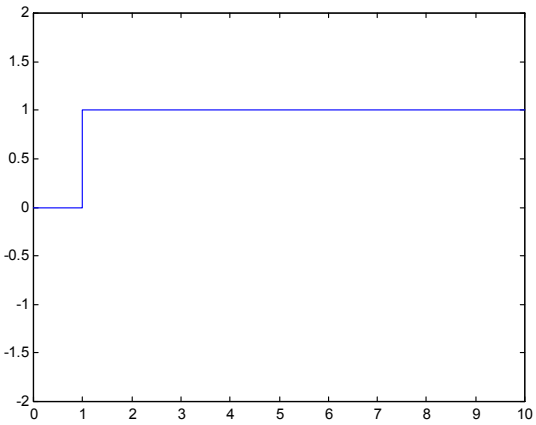

Fig. 23. Displacement command input.

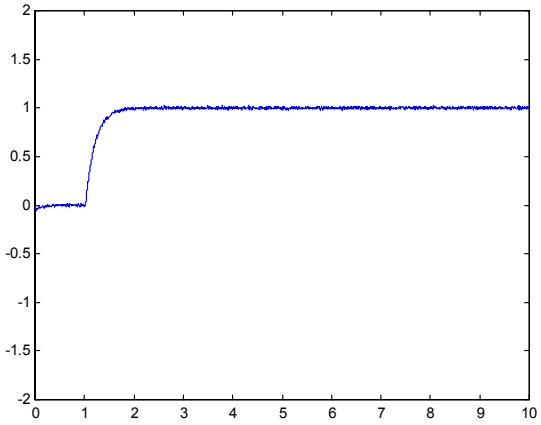

Fig. 24. Force response output by disturbance observer-based controller.

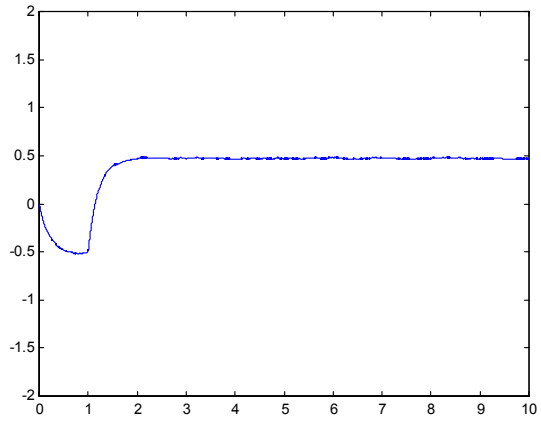

Fig. 25. Force response output by PD controller.

7. CONCLUSION

In this paper, the development of a medical tele-analyzer for abdominal mass analysis was presented. Overview of the developed system, hardware prototype, communication technique, and control algorithm were considered and implemented. Disturbance observer-based control was proposed to overcome disturbance occurred in the system. Displacement and force controls were investigated in hybrid scheme by both simulation and experiment. From the results, the proposed system was found to work well even with internal and external disturbances. Disturbance observer-based controller was compared with PD controller. There was no steady-state error in the former controller, while steady-state error was detected in the latter controller. In the future work, investigation of the effect of communication delay time to the system and development of medical tactile database are planned.

REFERENCES

[1] C. Baur, D. Guzzohi, and O. Georg, “VIRGY: A virtual reality and force force feedback based endoscopic surgery simulator,” *Stud Health*

Technol Inform, vol. 50, pp. 110-116, 1998.
[2] A. C. Dumay, "Medicine in virtual environments," *Technol Health Care,* pp. 75-89, 1995.
[3] L. D. Harmon, "Automated tactile sensing," *International Journal of Robotics Research,* vol. 1, no. 2, pp. 33-44, 1982.
[4] J. Y. S. Luh, W. D. Fisher, and R. P. C. Paul, "Joint torque control by a direct feedback for industrial robots," *IEEE Trans. on Automatic Control,* vol. AC28, no. 2, pp. 153-161, 1983.
[5] K. Ohnishi, "Robust motion control by disturbance observer," *Journal of Robotics and Mechatronics,* vol. 8, no. 3, pp. 218-225, 1996.
[6] M. Parnichkun, W. Po-ngaen, and T. Jearsiripongkul, "Development of a force-displacement controlled medical tele-analyzer," *Proc. of the IEEE International Symposium on Industrial Electronics,* Pusan, Korea, pp. 1978-1981, 2001.
[7] W. Po-ngaen, T. Jearsiripongkul, and M. Parnichkun, "Development of force-displacement hybrid controlled system for industrial tele-monitor and control," *Proc. of the International Conference on Production Research,* Bangkok Thailand, Conference CD-ROM, 2000.
[8] A. Suebsomran and M. Parnichkun, "Disturbance observer-based hybrid control of displacement and force in medical tele-analyzer for abdominal mass analysis," *Proc. of the IEEE International Conference on Industrial Technology,* Bangkok, pp. 365-369, 2002.

Anan Suebsomran received the M.Eng. degree in Mechatronics from Asian Institute of Technology in 1999. His research interests include mechatronics and robotics.

Manukid Parnichkun received the Ph.D. degree in Precision Machinery Engineering from the University of Tokyo in 1996. His research interests include mechatronics and robotics.